Available online at www.sciencedirect.com
SCIENCE DIRECT®
Journal of Sound and Vibration 287 (2005) 845–863
JOURNAL OF SOUND AND VIBRATION
www.elsevier.com/locate/jsvi

Buckling and vibration of circular cylindrical shells containing hot liquid

N. Ganesan*, V. Pradeep

Department of Applied Mechanics, Machine Dynamics Laboratory, Indian Institute of Technology Madras, Chennai, 600 036, India

Received 19 November 2003; received in revised form 20 November 2004; accepted 2 December 2004
Available online 2 February 2005

Abstract

Cylindrical shell filled with hot liquid is analyzed for buckling and vibration behavior using semi-analytical finite element method. A parametric study is conducted on a 316L stainless-steel cylinder filled with hot liquid. The temperature distribution in shell domain is obtained by using axisymmetric eight-node ring finite elements, capable of taking axial variation of temperature into account. Three-node ring elements are used for buckling and vibration analysis, formulated using semi-analytical finite element method. Thermal stress resultants and moment resultants in the shell are estimated and static buckling analysis is carried out to find the buckling temperature of the container for different levels of filling of liquid and for two different boundary conditions. Free vibration analysis carried out by considering initial stress effect and added mass effect due to hot liquid. Two different geometries are considered to study the effect of geometry on buckling temperature.

1. Introduction

Metallic containers find their application in nuclear industry for storing hot liquid for example, container vessels for storing liquid sodium in Liquid Metal Reactors (LMR) [1]. One among many of the primary requirements is the assessment of the buckling temperature and the natural

*Corresponding author. Tel.: +91 44 2351365; fax: +91 44 2350509.
E-mail address: nganesan@iitm.ac.in (N. Ganesan).

0022-460X/$ - see front matter © 2004 Elsevier Ltd. All rights reserved.
doi:10.1016/j.jsv.2004.12.001

Nomenclature

k	thermal conductivity of the material
$\dot{q}$	internal heat generated per unit volume
T	temperature inside the element
T_0	specified temperature on the surface S_1
l_r, l_z	directional cosines in respective directions
q,h	specified heat flux and heat transfer coefficients on the surface S_2
$[K_1^e]$	element conductivity matrix
$[K_2^e]$	element convective matrix
$[K_3^e]$	element capacitance matrix
ρ	density of the material of the structure
$[P_1^e]$	load vector due to $\dot{q}$
$[P_2^e]$	load vector due to q
$[P_3^e]$	load vector due to h
T_∞	ambient temperature
l	element edge length
C	2π if $m = 0$
	π if m $\succ$ 0
$[K_m]$	system stiffness matrix for harmonic 'm'
$[K_{Gm}]$	system geometric stiffness matrix for harmonic 'm'
$[M_m]$	system mass matrix for harmonic 'm'
$[M_{am}]$	system added mass matrix for harmonic 'm'
λ	buckling parameter

frequencies of the container. The container in the form of a cylinder is a popular choice. A detailed discussion on thermal buckling of thin cylindrical shells and columns subjected to uniform temperature rise, large temperature variation and time effects of creep can be found in the article by Hoff [2]. Hoff's paper also presents a survey of the solutions to problems falling under these heading. Abir and Nardo [3] considered the problem of thermal buckling of thin circular cylinders when there is a temperature gradient in circumferential direction. Lu and Chang [4] have studied the thermal buckling of conical shells when temperature varies along the generator. Thornton [5] has compiled an exhaustive review of thermal buckling of plates and shells. Amabili [6] studied analytically, the free vibrations of a circular cylindrical tank partially filled with inviscid incompressible fluid. Jayaraj et al. [7] proposed a new formulation using semi-analytical finite element method for elastic shells conveying fluids. To the best of author's knowledge no study has been reported on the buckling and vibration of cylindrical shells filled with hot liquids. In this present paper, thermal buckling temperatures and free vibration characteristics of a 316L stainless-steel cylinder filled with hot liquid are estimated taking into account the effect of thermally induced initial stresses, and the added mass effect due to the liquid present inside the container. The dimensions of the cylinder used for the analysis are same as those reported in the work of Lee et al. [1]. The analysis is based on decoupled thermo-mechanical and coupled fluid–structure interaction. First-order shear deformation theory is used to formulate structural finite element [8]. Axisymmetric Fourier heat conduction equation in cylindrical coordinates forms the basis for finite element formulation for evaluating temperature distribution. Eight-node axisymmetric elements are used in the shell domain for evaluating the temperature distribution along the length and thickness of the shell. The effect of thermally induced pre-stresses on the buckling and vibration behavior are studied incorporating the geometric stiffness matrix formulated by Ganesan and Kadoli [9].

The fluid domain analysis follows from Ross [10]. Numerical studies are carried out on two different shells having two different l/r ratios. The buckling behavior is investigated with respect to the amount of hot liquid contained in the cylindrical shell. Two different boundary conditions

are considered for buckling analysis, and the causes for buckling failure are examined. Vibration studies are carried out on the cylinder with liquid level as a parameter. The effect of liquid present inside the container on the frequency behavior is taken care by added mass matrix from Ross [10]. The lowest-frequency mode and the lowest buckling modes are found to be invariant with respect to the level of filling.

2. Semi-analytical finite element formulation for buckling and free vibration analysis of hot liquid-filled shell of revolution

In the present study, the buckling temperatures and the natural frequencies of the shell are solved using initial stability equation and equation of motion framed using the stiffness matrix, geometric stiffness matrix–mass matrix and added mass matrix. In the sections to follow, a detailed discussion on the semi-analytical finite element formulation for heat conduction analysis, buckling eigenvalue problem and free vibration equation of motion is presented. The buckling and frequency analyses are carried out by solving the corresponding eigenvalue problems.

2.1. Finite element formulation for temperature evaluation

The Fourier heat conduction equation for axisymmetric steady-state heat conduction with isotropic material properties is given by

$$\frac{1}{r}\left(\frac{\partial}{\partial r}\left(rk\,\frac{\partial T}{\partial r}\right)+\frac{\partial}{\partial z}\left(rk\,\frac{\partial T}{\partial z}\right)\right)+\rho\dot{q}=0 \tag{1}$$

with the boundary conditions

$$T=T_0(r,z)\ \text{ on surface }\ S_1,\ \text{ and}$$

$$k\,\frac{\partial T}{\partial r}\,l_r+k\,\frac{\partial T}{\partial z}\,l_z+q+h(T-T_\infty)=0\ \text{ on surface }\ S_2,$$

where the surfaces S_1 is the surface on which temperature is specified and S_2 is a surface on which convection and flux are specified. The problem defined in Eq. (1) along with the associated boundary conditions can be represented by equivalent functional expression [11] as follows:

$$I=\frac{1}{2}\int_v\left\{\begin{matrix}\dfrac{\partial T}{\partial r}\\[2mm]\dfrac{\partial T}{\partial z}\end{matrix}\right\}^{\mathrm{T}}\begin{bmatrix}k & 0\\ 0 & k\end{bmatrix}\left\{\begin{matrix}\dfrac{\partial T}{\partial r}\\[2mm]\dfrac{\partial T}{\partial z}\end{matrix}\right\}2\pi r\,\mathrm{d}r\,\mathrm{d}z+\int_v\rho qT2\pi r\,\mathrm{d}r\,\mathrm{d}z$$
$$+\frac{1}{2}\int_{s_2}hT^2 2\pi r\,\mathrm{d}S_2-\int_{s_2}hTT_\infty 2\pi r\,\mathrm{d}S_2+\int_{s_2}qT2\pi r\,\mathrm{d}S_2. \tag{2}$$

Eq. (2) represents the variational expression of the governing equation stated in Eq. (1). The natural boundary condition (convection and flux) are contained in the variational expression itself. The essential boundary conditions (temperature specification) are to be applied after forming the global finite element matrices. The temperature T can be expressed in terms of nodal temperatures T_i by using shape functions N_i as $T = \sum_{i=1}^{p} T_i N_i$, where p is the number of nodes per element. By substituting the expression for T in the functional expression (2) and minimizing the functional with respect to the nodal variables T_i, the following elemental matrix equation can be obtained:

$$[K_1^e]T^e + [K_2^e]T^e = [P^e], \quad \text{where } [P^e] = [P_1^e] + [P_2^e] + [P_3^e]. \tag{3}$$

For a shell of revolution neglecting heat transfer from the edges of the shell and transforming r, z into natural coordinates the above matrices will be

$$[K_1^e] = 2\pi \int \int [B]^{\mathrm{T}}[K][B] r(\xi,\eta)|J| \, \mathrm{d}\xi \, \mathrm{d}\eta,$$

$$[K_2^e] = 2\pi \int h[N]^{\mathrm{T}}[N] r(\xi,\eta) \frac{l}{2} \, \mathrm{d}\xi,$$

$$[P_1^e] = 2\pi \int \int \dot{q}[N]^{\mathrm{T}} r(\xi,\eta)|J| \, \mathrm{d}\xi \, \mathrm{d}\eta,$$

$$[P_2^e] = 2\pi \int q[N]^{\mathrm{T}} r(\xi,\eta) \frac{l}{2} \, \mathrm{d}\xi,$$

$$[P_3^e] = 2\pi \int hT_\infty[N]^{\mathrm{T}} r(\xi,\eta) \frac{l}{2} \, \mathrm{d}\xi.$$

$r(\xi,\eta) = \sum_{i=1}^{n} N_i r_i$ is the radius at the Gaussian point (ξ,η). The final system matrices can be obtained by assembling the element matrices. Eight-noded ring elements with one dof per node are formulated for descretizing the shell domain for temperature evaluation. The element geometry and the directions of natural coordinates (ξ,η) are depicted in Fig. 1.

2.2. Finite element formulation for liquid-filled container considering initial stress effect due to temperature

2.2.1. First-order shear deformation theory (FSDT)

In the FSDT in contrast to thin shell theory, the thickness of the shells is comparable to the least radius of curvature. The geometry of a shell of revolution is depicted in Fig. 2. Rao [8] studied the dynamic and static characteristics of laminated beams and shells of revolution and compares different order shear deformation theories.

The surface generated by revolving the generating curve is the reference surface and the thickness coordinate is measured from this surface along the normal to the surface at a given

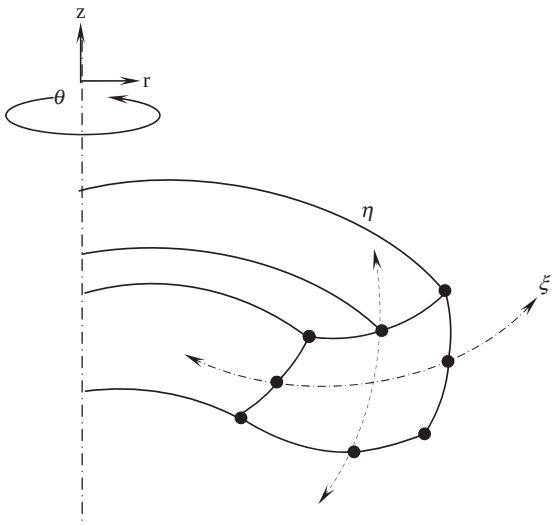

Fig. 1. Eight-node ring element with the coordinate systems.

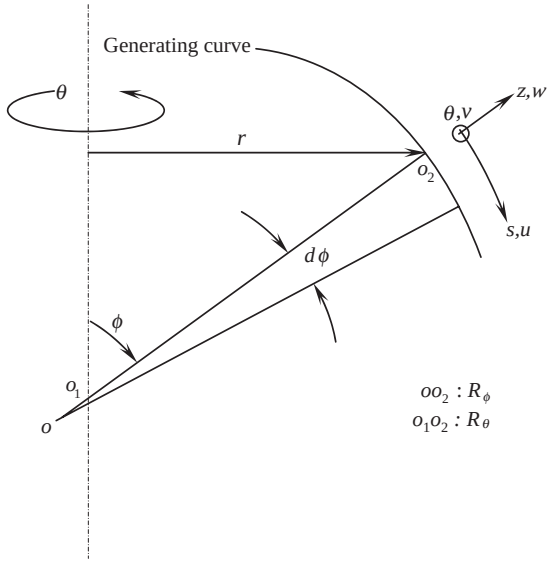

Fig. 2. Geometry of a shell of revolution.

point. In case of shell of uniform thickness this surface can be taken to be the middle surface where ($z = 0$) and the thickness coordinates of top and bottom surfaces are given by $z = t/2$ and $-t/2$, respectively (t is the shell thickness.). In this theory the displacement field in the shell domain is expressed in terms of the middle surface displacements u_0, v_0, and w_0 (displacements along the s, θ, and z directions, respectively) and the rotations of the normal to the middle surface of the shell, Ψ_s, Ψ_θ (rotations in the s and θ, directions, respectively). The displacements u, v, and w in

the s, θ, and z directions are given by

$$u(s,\theta,z) = u_0(s,\theta) + z\Psi_s,$$
$$v(s,\theta,z) = v_0(s,\theta) + z\Psi_\theta,$$
$$w(s,\theta,z) = w_0(s,\theta), \tag{4}$$

where z is the radial coordinate measured from the middle surface of the shell.

The strain-displacement relations according to FSDT are given by

$$\varepsilon_{ss} = \frac{1}{A_1}(\varepsilon^0_{ss} + zk^1_s),$$
$$\varepsilon_{\theta\theta} = \frac{1}{A_2}(\varepsilon^0_{\theta\theta} + zk^1_\theta),$$
$$\gamma_{s\theta} = \frac{1}{A_1A_2}(\gamma^0_{s\theta} + zk^1_{s\theta}),$$
$$\gamma_{\theta z} = \frac{1}{A_2}\gamma^0_{\theta z},$$
$$\gamma_{sz} = \frac{1}{A_2}\gamma^0_{sz}, \tag{5}$$

$A_1 = 1 + z/R_\phi$ and $A_2 = 1 + z/R_\theta$.

R_θ and R_φ are the radii of curvatures in respective directions. $\varepsilon_{ss}, \varepsilon_{\theta\theta}, \gamma_{s\theta}, \gamma_{\theta z}, \gamma_{sz}$ are the strains at any point in the shell, expressed in terms of the strains in the middle surface of the shell $\varepsilon^0_{ss}, \varepsilon^0_{\theta\theta}, \gamma^0_{s\theta}, \gamma^0_{\theta z}, \gamma^0_{sz}$ and the change in curvatures $\kappa^1_s, \kappa^1_\theta, \kappa^1_{s\theta}$.

2.2.2. Structural stiffness matrix

The total strain energy U, in the continuum is

$$U = U_1 + U_2. \tag{6}$$

U_1 is the conventional strain energy due to deformation of the structure and U_2 is strain energy due to initial stresses in the structure. The structural stiffness matrix is obtained from the expression for U_1 given by

$$U_1 = \frac{1}{2}\int_v \{\varepsilon_{ss}\sigma_{ss} + \varepsilon_{\theta\theta}\sigma_{\theta\theta} + \gamma_{\theta z}\tau_{\theta z} + \gamma_{sz}\tau_{sz} + \gamma_{s\theta}\tau_{s\theta}\}\,\mathrm{d}V$$
$$= \frac{1}{2}\int_v \{\varepsilon\}^{\mathrm{T}}\{\sigma\}\,\mathrm{d}V, \tag{7}$$

$$\{\varepsilon\}^{\mathrm{T}} = \{\varepsilon_{ss}\ \varepsilon_{\theta\theta}\ \gamma_{\theta z}\ \gamma_{sz}\ \gamma_{s\theta}\} \text{ are strains}$$

$$\{\sigma\}^{\mathrm{T}} = \{\sigma_{ss}\ \sigma_{\theta\theta}\ \tau_{\theta z}\ \tau_{sz}\ \tau_{s\theta}\} \text{ are the corresponding stresses in respective directions.}$$

Expressing the strains and stress in terms of middle surface strains $\varepsilon^0_{ss}, \varepsilon^0_{\theta\theta}, \gamma^0_{s\theta}, \gamma^0_{\theta z}, \gamma^0_{sz}$, and the change in curvatures $\kappa^1_s, \kappa^1_\theta, \kappa^1_{s\theta}$, and then performing explicit integration in z direction, the

expression for U_1 becomes

$$U_1 = \frac{1}{2}\int_A \{\varepsilon_0\}^{\mathrm{T}}\{\hat{N}\}\,\mathrm{d}A.$$

$\{\varepsilon_0\}^{\mathrm{T}}$ and $\{\hat{N}\}^{\mathrm{T}}$ are the generalized strain vector and array of stress resultants, respectively, defined as

$$\{\varepsilon_0\}^{\mathrm{T}} = \{\varepsilon^0_{ss}\ \varepsilon^0_{\theta\theta}\ \gamma^0_{s\theta}\ \kappa^1_s\ \kappa^1_\theta\ \kappa^1_{s\theta}\ \gamma^0_{sz}\ \gamma^0_{\theta z}\},$$

$$\{\hat{N}\}^{\mathrm{T}} = \{N_{ss}\ N_{\theta\theta}\ N_{s\theta}\ M_{ss}\ M_{\theta\theta}\ M_{s\theta}\ Q_s\ Q_\theta\}.$$

The stress resultants $\{\hat{N}\}$ can be expressed in terms of generalized strains as

$$\{\hat{N}\} = [D]\{\varepsilon_0\}.$$

$[D]$ is the constitutive matrix. In the semi-analytical finite element method middle surface displacements u_0, v_0, and w_0 and the rotations Ψ_s, and Ψ_θ are expanded in Fourier series in circumferential direction as follows:

$$\begin{Bmatrix} u_0 \\ v_0 \\ w_0 \\ \Psi_s \\ \Psi_\theta \end{Bmatrix} = \sum_{m=0}^{\infty} \begin{bmatrix} \cos m\theta & 0 & 0 & 0 & 0 \\ 0 & \sin m\theta & 0 & 0 & 0 \\ 0 & 0 & \cos m\theta & 0 & 0 \\ 0 & 0 & 0 & \cos m\theta & 0 \\ 0 & 0 & 0 & 0 & \sin m\theta \end{bmatrix} \begin{Bmatrix} u_{0m} \\ v_{0m} \\ w_{0m} \\ \Psi_{sm} \\ \Psi_{\theta m} \end{Bmatrix} \tag{8}$$

'm' stands for mth circumferential harmonic.

Substituting the above expression (8) in the expression for $\{\varepsilon_0\}$ given in Ref. [8] and by making use of shape functions [8] the following expression can be obtained:

$$\{\varepsilon_0\} = [B]\{d\}. \tag{9}$$

$[B]$ is the strain-displacement matrix. The matrix $\{d\}$ will be $\{d\} = [[d_1]\ [d_2]\ [d_3]]^{\mathrm{T}}$, $[d_i] = (u_{0i}\ v_{0i}\ w_{0i}\ \Psi_{si}\ \Psi_{\theta i})^{\mathrm{T}}$ $i = 1, 2, 3$ are the dof corresponding to node i. The expression for stiffness matrix is given by

$$[K^*_e] = \int_A [B]^{\mathrm{T}}[D][B]\,\mathrm{d}A.$$

By carrying explicit integration in θ direction, each harmonic can be decoupled. The elemental stiffness matrix for harmonic 'm' is given by

$$[K^*_{em}] = C\int_\xi [B_m]^{\mathrm{T}}[D][B_m]|J|\,\mathrm{d}\xi, \tag{10}$$

$$\begin{aligned} C &= 2\pi \quad \text{if } m = 0, \\ &= \pi \quad \text{if } m \succ 0, \end{aligned} \qquad |J| \text{ is the jacobian}$$

and the expressions for $[B_m], [D]$ are given in Ref. [8].

2.2.3. Mass matrix

The mass matrix is obtained from the kinetic energy expression for the shell continuum.

The kinetic energy

$$\mathrm{KE} = \frac{\rho}{2}\int_A \{\dot{d}_e\}^{\mathrm{T}}[M_e]\{\dot{d}_e\}\,\mathrm{d}A. \tag{11}$$

Expressing the expression (11) in terms of generalized coordinates, making use of the shape functions [8] and by carrying explicit integration in the thickness direction the kinetic energy will become

$$\mathrm{KE} = \frac{1}{2}\int_A \{\dot{d}_e\}^{\mathrm{T}}[M_e]\{\dot{d}_e\}\,\mathrm{d}A.$$

The elemental mass matrix $[M_e]$ is given by

$$[M_e] = \rho\int_A \bar{N}^{\mathrm{T}}\bar{N}\,\mathrm{d}A.$$

By carrying explicit integration in θ direction, each harmonic can be decoupled. The elemental mass matrix for harmonic 'm' is given by

$$[M_{em}] = \rho C\int_\xi [\bar{N}_m]^{\mathrm{T}}[\bar{N}_m]|J|\,\mathrm{d}\xi, \tag{12}$$

$[\bar{N}_m]$ is the shape function matrix.

2.2.4. Thermal load vector

The elemental thermal load vector for harmonic 'm' can be written as

$$[F^e_{\mathrm{Th}}] = C\int_\xi [B_m]^{\mathrm{T}}[\bar{D}][\varepsilon^i_0]|J|\,\mathrm{d}\xi. \tag{13}$$

$[\varepsilon^i_0]$ are the strains due to free thermal expansion. By solving the problem $[K_m][\delta_i] = [F_{\mathrm{Th}}]$, the initial nodal displacements $[\delta_i]$ are obtained. By using $[\delta_i]$ the initial thermal stress resultants are found for generating the geometric stiffness matrix.

2.2.5. Geometric stiffness matrix

The expression for geometric stiffness matrix can be obtained from the expression for U_2 given by

$$U_2 = \frac{1}{2}\int_V (\varepsilon^n_{ss}\ \ \varepsilon^n_{\theta\theta})\begin{bmatrix}\sigma^i_{ss} & \tau^i_{s\theta}\\ \tau^i_{s\theta} & \sigma^i_{\theta\theta}\end{bmatrix}\begin{pmatrix}\varepsilon^n_{ss}\\ \varepsilon^n_{\theta\theta}\end{pmatrix}\mathrm{d}V, \tag{14}$$

$\varepsilon^n_{ss}, \varepsilon^n_{\theta\theta}$ are the nonlinear strains and $\sigma^i_{ss}, \sigma^i_{\theta\theta}, \tau^i_{s\theta}$ are the initial stresses. These initial stresses can be found by solving static problem with thermal load. U_2 can be written in terms of initial stress resultants and generalized nonlinear strains. Then the expression for U_2 becomes

$$U_2 = \frac{1}{2}\int_A \{d\}^{\mathrm{T}}[K_G]\{d\}\,\mathrm{d}A,$$

$[K_G]$ is the geometric stiffness matrix. The expression for $[K_G]$ is given by

$$\left[K_G^e\right] = \int_A \left[\widehat{B}\right]^{\mathrm{T}} \left[\widehat{D}\right] \left[\widehat{B}\right] \mathrm{d}A.$$

$[\widehat{B}]$ is the nonlinear strain-displacement matrix, formed by making use of the nonlinear strains. Due to the orthogonality property the matrix $[K_G]$ can be decoupled for each harmonic. The geometric stiffness matrix for harmonic 'm' can be written as

$$\left[K_{Gm}^e\right] = C \int_\xi \left[\widehat{B}_m\right]^{\mathrm{T}} \left[\widehat{D}\right] \left[\widehat{B}_m\right] |J| \, \mathrm{d}\xi. \tag{15}$$

The expressions for $[K_{Gm}^e][\widehat{D}]$ and $[\widehat{B}_m]$ are given in Ref. [9].

2.2.6. Added mass matrix

Due to the liquid present in the container the frequency of the structure decreases. The final system 'added mass' matrix for harmonic 'm' is given by Ross [10].

$$[M_a] = \frac{C}{\rho_f} [S_m]^{\mathrm{T}} [H_m]^{-1} [S_m]. \tag{16}$$

$[S_m]$ and $[H_m]$ are the interaction matrix and compression energy matrix, respectively. The elemental interaction matrix $[S_m^e]$ and elemental compression energy matrix $[H_m^e]$ are given by

$$[S_m^e] = C\rho_f \int_s [N]^{\mathrm{T}} [\bar{N}] \, \mathrm{d}S,$$

$$[H_m^e] = C \int_A \left[\vec{B}\right]^{\mathrm{T}} \left[\vec{B}\right] \mathrm{d}A.$$

All the other system matrices can be obtained by assembling the elemental matrices.

3. Results and discussion

A finite element computer code is developed using eight-node axisymmetric ring finite elements for evaluating temperature distribution in the shell domain. The code developed is validated for temperature evaluation with the example in Ref. [12]. For buckling and vibration analysis code developed by Ganesan and Kadoli [9] is used, which is already validated.

3.1. Validating the thermal code

The code is validated for two different thickness of a long hollow circular cylinder, to study the effect of thickness of the shell on the temperature distribution across the thickness of the shell. Consider an infinitely long hollow circular cylinder as shown in the Fig. 3(a) the inside surface of the tube has a distributed heat flux of $q = 200$ acting on it, where as the outside surface is subjected to convection with convective heat transfer coefficient $\beta = 5$ and $T_\infty = 30$. The thermal conductivity of the material of the tube is $k = 3$. As the temperature does not vary axially or circumferentially, FE solution is obtained by using just one element in axial direction and '8'

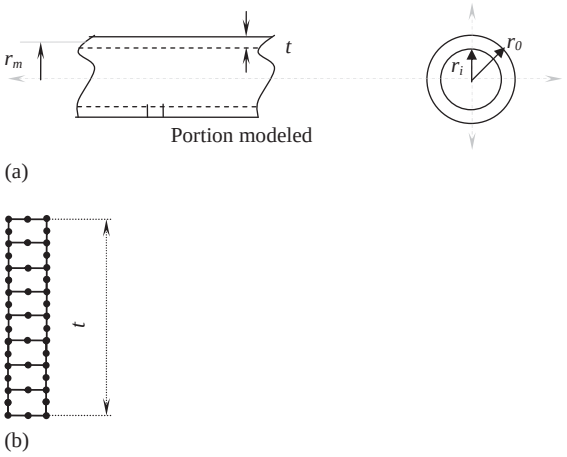

Fig. 3. (a) Infinitely long hollow cylinder and (b) finite element mesh used for modeling.

eight-node elements in thickness direction as shown in the Fig. 3(b). Here, we consider two different tube thicknesses. (a) $t = 18(r_m/t = 0.55556)$ and (b) $t = 0.1(r_m/t = 100)$. Any consistent system of units can be made use of.

The analytical solution for the above problem is given by Surana and Orth [12] Eq. (17)

$$(T)_{\text{theory}} = \frac{qr_i}{K}\left[\ln\left(\frac{r_0}{r}\right) + \frac{k}{\beta r_0}\right] + T_\infty. \tag{17}$$

The plots shown in the Fig. 4 compare the finite element and analytical solutions for the two different cases considered. It can be seen that there is a good agreement between FE and analytical solutions. Hence, computer code developed for temperature evaluation is validated. It can be seen that the variation of the temperature across the thickness is second order in case of larger wall thicknesses and it is linear in case of shells having thin walls.

3.2. Buckling analysis

For carrying out the buckling analysis and estimating the buckling temperature, the temperature distribution in the shell domain is evaluated first. Then the induced thermal stresses are calculated to evaluate the geometric stiffness matrix. The following eigen value problem:

$$[[K_m] + \lambda[K_{Gm}]][X] = 0 \tag{18}$$

is solved for evaluating the buckling temperature. The dimensions of the cylinder used for the analysis are shown in Fig. 5(a) along with the associated thermal boundary conditions. The cylinder is filled with hot liquid sodium at 550 °C up to the level indicated in the figure. On the outer and inner (surface above liquid interface) surfaces of the shell, a convective heat transfer coefficient of 6.5 W/m^2 and an ambient temperature of 15 °C is assumed. Constant temperature boundary condition (equal to temperature of the liquid inside) will prevail on the surface in contact with the liquid. Fig. 5(b) shows the finite element mesh used for evaluating the temperature. Fifty two elements are used in axial direction, and only one element in thickness direction. For the materials having high thermal conductivity, such as a one used in the present

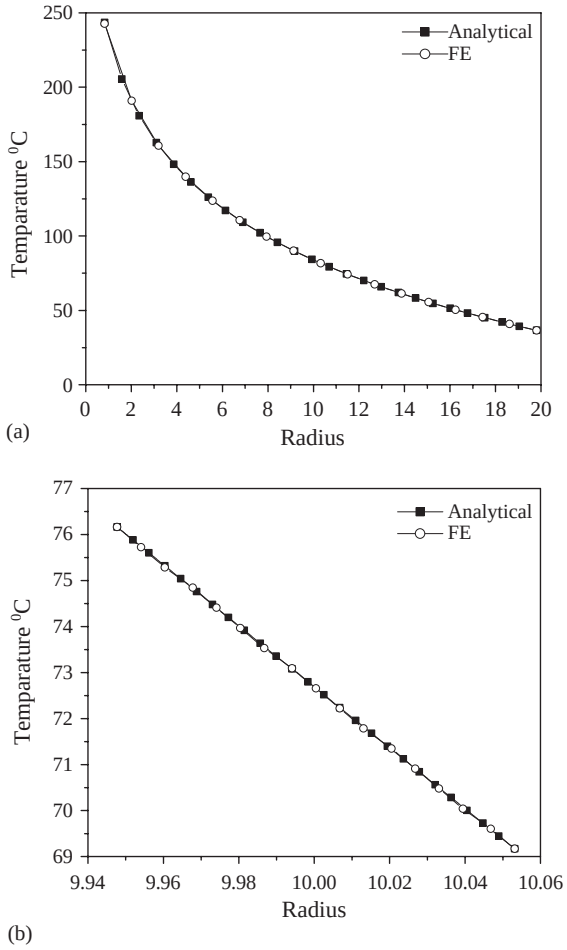

Fig. 4. Comparison of finite element solution with analytical solution (a) ($r_m/t = 0.55556$) and (b) ($r_m/t = 100$) (r_m is the mean radius of the cylinder).

analysis almost constant temperature prevails along the thickness direction. So nodal temperatures on the middle line of the thickness of the shell are used for further calculations.

Fig. 6 shows the temperature distribution along the length of the shell for four levels of filling of hot liquid sodium at 550 °C. The distribution has a break at the liquid level, up to which it remains constant at the liquid temperature. In the remaining portion of the length there is a second-order variation of temperature. The distribution curve becomes asymptotic at the end, and tends to a constant value. The value of this constant depends on the level of the liquid. Since shell is very thin (3 mm) the temperature drop across the thickness will be negligible for the case of thermal boundary conditions we considered. For other boundary conditions (say for example temperature specification on outer surface instead of convection) this assumption may not be valid.

Fig. 7 shows the finite element discretization of the shell domain for buckling analysis. Three-node ring elements are used for the shell domain.

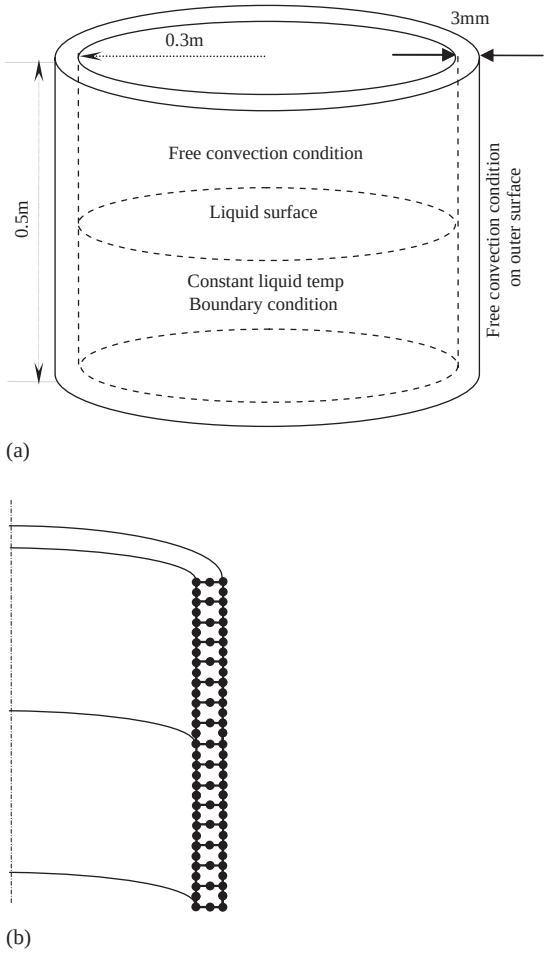

Fig. 5. (a) Dimensions of the container used for analysis [1] along with the thermal boundary conditions and (b) finite element mesh used for evaluation of temperature.

The nodal temperatures obtained from the previous calculations (at a reference liquid temperature (T_{ref})) are used for the buckling and vibration analysis. The thermally induced pre-stresses hence the geometric stiffness matrix $[K_G]$ are evaluated at this liquid temperature. For the evaluation of buckling temperature. The eigen value problem (18) is solved for a reference temperature T_{ref} and the value $T_b = \lambda * T_{\text{ref}}$ gives the buckling temperature of the shell. Table 1 lists the buckling temperatures of the cylinder for four different levels of liquid filling for clamped–clamped boundary condition and for different circumferential modes. All the dof, namely displacements u_0, v_0, and w_0 and the rotations Ψ_s, and Ψ_θ at both the ends of the shell are constrained. As the level of the liquid increases the value of buckling temperature decreases as expected. The mode (9, 1) is the lowest buckling temperature mode.

It is necessary to investigate the determining factor for the buckling failure of the system. Fig. 8 shows the axial and hoop stress resultants induced in the cylinder for four different levels of filling

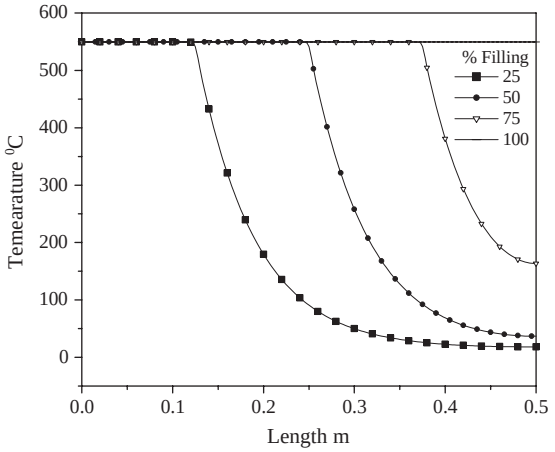

Fig. 6. Temperature distribution along the length of the shell for different levels of liquid filling.

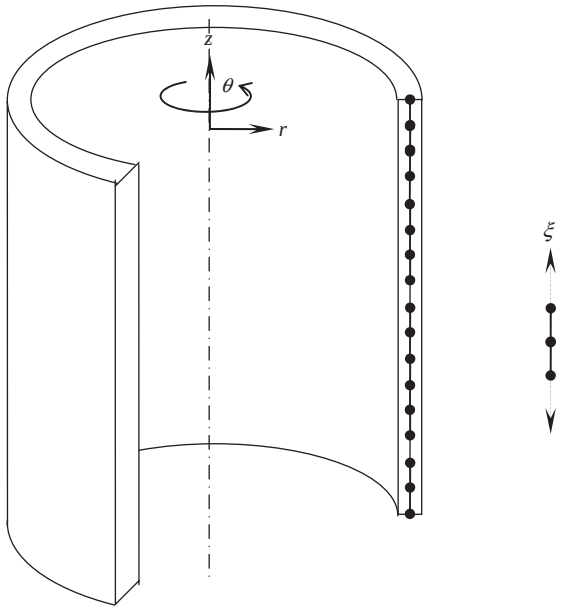

Fig. 7. Finite element mesh used for buckling analysis.

for clamped–clamped boundary condition. The stress resultants are calculated at the buckling temperature of the liquid for the given level of filling. It can be seen that at buckling temperature the axial stress resultant reaches a constant value for all the liquid level and buckling is due to axial compression.

Table 2 lists the minimum buckling temperatures and corresponding circumferential modes for four different levels of liquid filling and for clamped-simply supported boundary condition. Displacements v_0, and w_0 and the rotation Ψ_θ are constrained at the simply supported edge. It can

Table 1
Buckling temperatures of a clamped–clamped container

Buckling mode	T_b (°C) for fraction filling			
	0.25	0.50	0.75	1.0
1	1014	610	448	391
2	1012	609	447	391
3	1010	607	446	390
4	1007	605	444	389
5	1004	603	442	387
6	1000	601	441	385
7	983	597	438	383
8	955	591	435	380
9	935	580	430	375
10	936	585	436	382
11	950	611	457	401
12	975	647	488	429
13	1006	685	524	463
14	1041	726	564	500
15	1078	768	605	540

Radius = 0.3 m and length = 0.5 m.

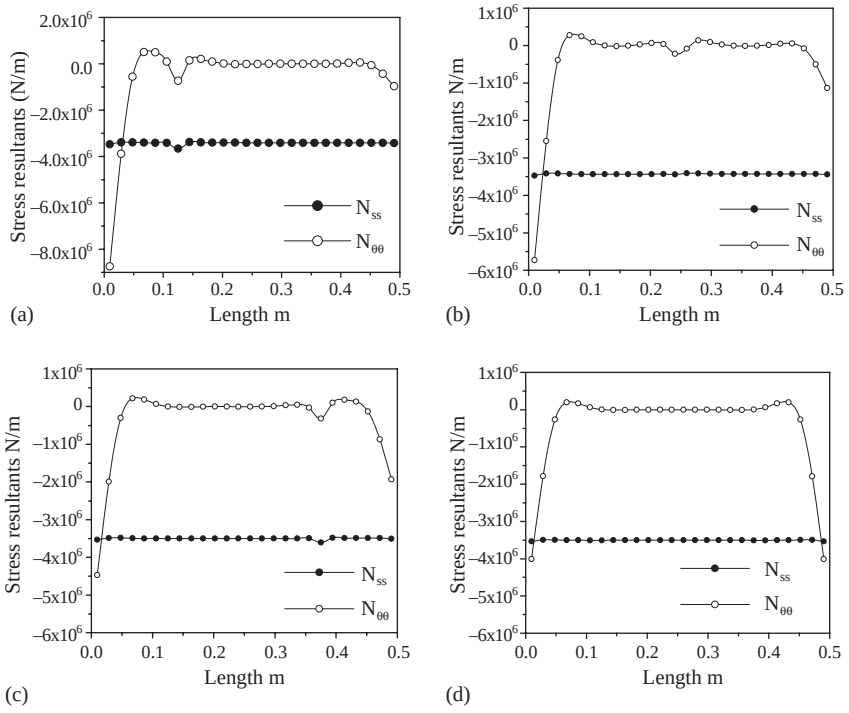

Fig. 8. Thermal stress resultants induced in the cylinder with clamped–clamped boundary condition at buckling temperature for fraction filling (a) 0.25 (b) 0.50 (c) 0.75 (d) 1.00.

Table 2
Buckling temperatures of a clamped-simply supported cylindrical shell

Lowest buckling mode	T_b (°C) for fraction filling			
	0.25	0.50	0.75	1.0
(20,1)	2259	2236	2236	2236

Radius = 0.3 m, length = 0.5 m.

Table 3
Buckling temperatures of a clamped-simply supported cylindrical shell

Lowest buckling mode	T_b (°C) for fraction filling	
	0.50	1.0
(20,1)	2206.9580	2206.9580

Radius = 0.3 m, length = 1.5 m.

be observed that buckling temperature is almost invariant with the level of hot liquid. Table 3 shows the buckling temperature for a cylinder having the same radius as the one considered but having a length of 1.5 m. For this cylinder buckling temperatures are evaluated for two levels of filling for clamped-simply supported boundary condition. Again there is no change in buckling temperatures is observed with the change in the level of liquid filling as can be seen from Table 3.

Fig. 9 shows the stress distributions along the length of the shell with clamped-simply supported boundary condition, for two different levels of filling. The temperature of the liquid inside is 550 °C. The plots show the same value of maximum compressive hoop stress resultant at the clamped end for both the cases. At the other end the value of this stress resultant is less. Thus, buckling is due to hoop compression for this boundary condition.

3.3. Frequency behavior

Fig. 10 shows the finite element mesh of the hot liquid-filled container for frequency analysis. Eight-node ring elements are used for the fluid domain and three-node ring elements are used for discretizing the structural domain. A similar study on fluid-filled cylinders was done by Amabili [13] considering the effect of free surface waves and the sloshing modes can be captured by such an approach. In contrast, in the present study rigid free surface boundary condition is assumed.

For analyzing the frequency behavior of the system considered, it is important to consider two effects which alter the natural frequencies of the system namely the 'added mass effect', due to the liquid present inside, and the 'initial stress effect' due to the induced thermal stresses in the container because of the high temperature of the liquid inside. The added mass adds to the system mass matrix in the form of added mass matrix $[M_a]$, and lessens the effective frequency. Initial stress effect is accounted by the geometric stiffness matrix $[K_G]$, and the frequency behavior is altered due to the altered stiffness. The eigen value problem given by Eq. (19) is solved for

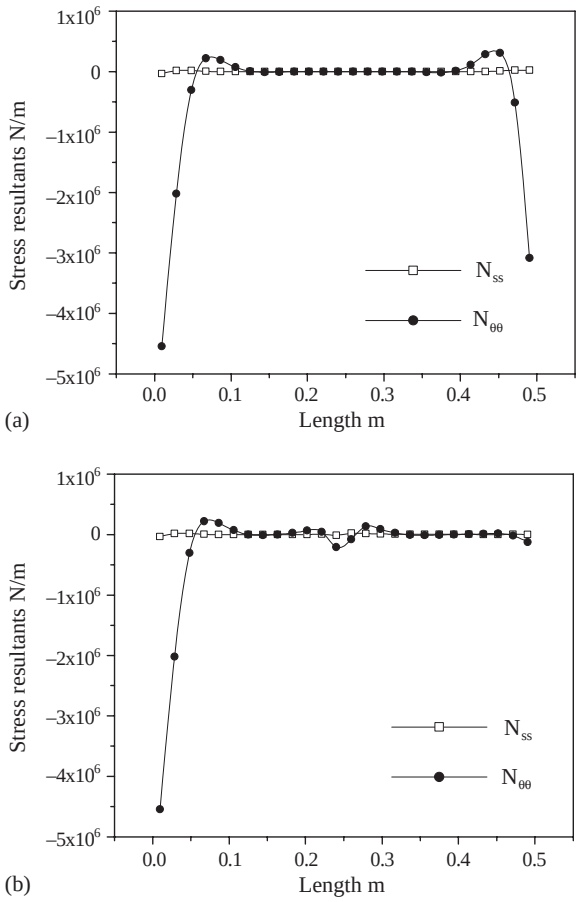

Fig. 9. Thermal stress resultants induced in the cylinder with clamped simply supported boundary condition at 550 °C for fraction filling (a) 1 (b) 0.5.

obtaining the natural frequencies ω and the natural modes.

$$[[[K_m] + [K_{Gm}]] - \omega^2[[M_{am}] + [M_m]]][X] = 0. \tag{19}$$

Fig. 11(a) and (b) shows the natural frequency variation of the first axial mode for different circumferential modes with temperature. It can be observed that (6,1) is the lowest-frequency mode initially. As the temperature increases there is a cross over of (6,1) and (9,1) modes after which (9,1) becomes lowest-frequency mode for all the levels of filling. Finally the shell buckles in (9,1) mode at a temperature where the natural frequency will become zero. This is the buckling temperature. As the temperature of the liquid increases the natural frequency of the shell goes on decreasing due to increase in its 'folding' tendency. It should be noted that the lowest frequency mode need not coincide with the first buckling mode. For a given boundary condition it is interesting to note that, for any level of liquid filling the buckling occurs in the same mode. The plots 3.9(c) and (d) shows the variation of frequency considering only the effect of thermally induced pre-stresses.

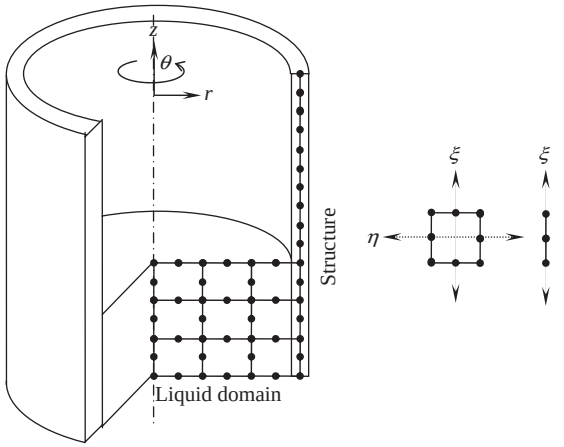

Fig. 10. Finite element discretization of the liquid-filled container for frequency analysis.

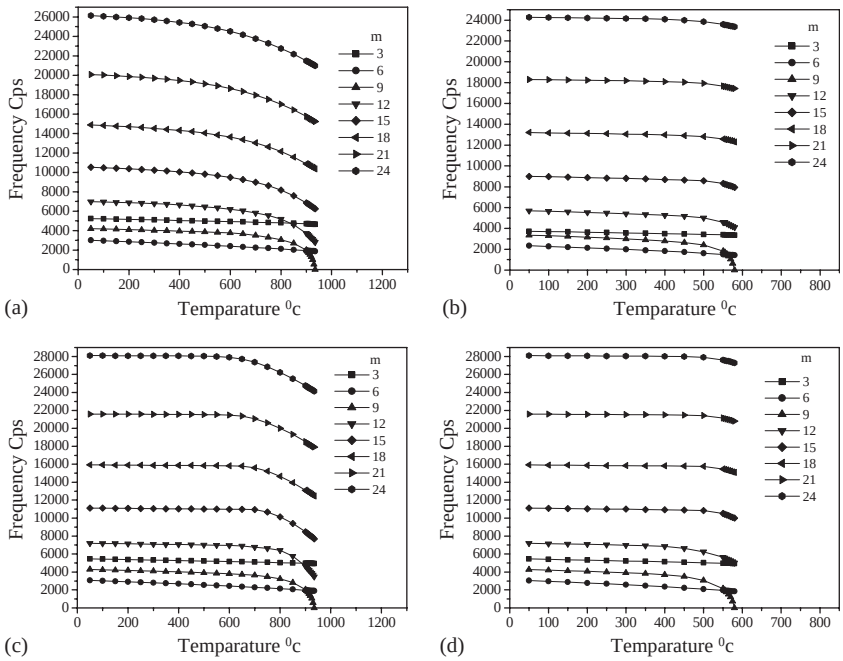

Fig. 11. Frequency behavior of the shell for two levels of filling (a) 0.25 (b) 0.5 with clamped–clamped boundary conditions. (c) and (d) indicate the effect of initial stresses alone.

Fig. 12(a) shows the variation of natural frequency of (9,1) mode with temperature. It can be observed that the combined added mass and initial stress effects are more in initial levels of filling. This is due to the fact that temperature profiles along the length of the shell do not deviate much from one another at higher levels of filling. So are the stress distributions, and so is the frequency behavior. The frequency in the (9,1) mode goes on decreasing with temperature and becomes zero

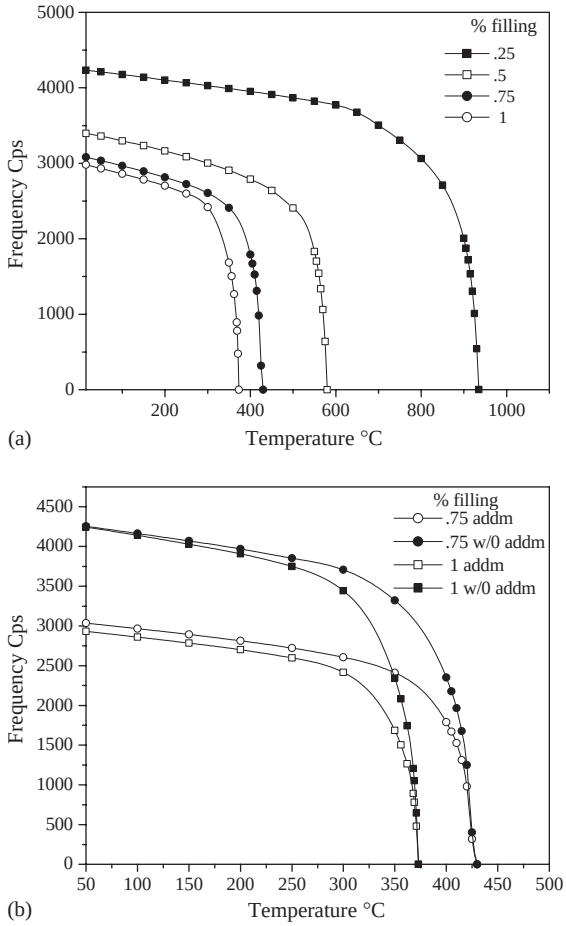

Fig. 12. (a) Variation of (9, 1) mode frequency with temperature for the levels of filling indicated, for clamped–clamped boundary condition and (b) comparison of initial stress effect alone and the actual frequency behavior of (9, 1) mode, for clamped–clamped boundary condition.

at buckling temperature Fig. 12(b) compares the effect of initial stress effect alone (w/o aadm) and the actual behavior (addm) of the shell.

4. Conclusions

A computer program is developed by making use of semi-analytical finite element method, capable of taking axisymmetric temperatures and temperatures may vary in axial direction. The code can take care of transient behavior of the system also. Buckling temperatures are evaluated for the containers for different levels of filling of the hot liquid and causes for the buckling failures were investigated. The changed natural frequencies of the shell are calculated due to added mass effect and initial stress effect. The effects of added mass and initial stresses on the first buckling mode are studied. The nature of the stress resultants is compared for two different boundary conditions.

References

[1] H.Y. Lee, J.B. Kim, J.H. Lee, Thermal ratcheting deformation of a 316L stainless steel cylindrical structure under an axial moving temperature distribution, *Journal of Pressure Vessels and Piping* 80 (2003) 41–48.
[2] N.J. Hoff, Buckling at high temperature, *Journal of Royal Aeronautic Society* 61 (1957) 756–774.
[3] D. Abir, A. Noda, Thermal buckling of circular cylindrical shells under the circumferential temperature gradients, *Journal of Aerospace Science* 26 (1959) 803–808.
[4] S.Y. Lu, L.K. Chang, Thermal buckling of conical shells, *AIAA Journal* 5 (10) (1967) 1877–1882.
[5] E. Thornton, Thermal buckling of plates and shells, *Applied Mechanics Review* 46 (10) (1993) 485–506.
[6] M. Amabili, Shell-plate interaction in the free vibrations of circular cylindrical tanks partially filled with a liquid: the artificial spring method, *Journal of Sound and Vibration* 99 (3) (1997) 431–452.
[7] K. Jayaraj, N. Ganesan, P. Chandramouli, A semi-analytical coupled finite element formulation for shells conveying fluids, *Computers and Structures* 80 (2002) 271–286.
[8] R.S. Rao, Static and dynamic problems in laminated beams and axisymmetric shells, Ph.D. Thesis, Indian Institute of Technology Madras, 1997.
[9] N. Ganesan, R. Kadoli, Buckling and dynamic analysis of piezothermoelastic composite cylindrical shell, *Journal of Composite Structures* 59 (2003) 45–60.
[10] C.T.F. Ross, *Pressure Vessels Under External Pressure: Statics and Dynamics*, Elsevier Applied Science, London, New York, 1994.
[11] K.S. Surana, P. Kalim, Isoparametric axisymmetric shell elements with temperature gradients for heat conduction, *Computers and Structures* 23 (2) (1986) 279–289.
[12] K.S. Surana, N.J. Orth, Axisymmetric shell elements for heat conduction with *p*-approximation in the thickness direction, *Computers and Structures* 33 (3) (1989) 689–705.
[13] M. Amabili, Axisymmetric shell elements for heat conduction with *p*-approximation in the thickness direction, *Computers and Structures* 33 (3) (1989) 689–705.